FE/SPH modelling of orthogonal micro-machining of f.c.c. single crystal

S.Abolfazl Zahedi, Murat Demiral, Anish Roy*, Vadim V. Silberschmidt

Wolfson School of Mechanical and Manufacturing Engineering, Loughborough University, LE11 3TU UK

*Corresponding author. Tel.: +44 1509 227637; Fax: +44 1509 227648
E-mail: A.Roy3@lboro.ac.uk

Abstract

With an increased use of mechanical micro-machining in manufacture of small-sized components with complex geometries, the need to understand mechanics of machining at micro-scale is recognized. Numerical modelling is a powerful tool which can be used to gain insight into the underlying mechanisms that drive a plastic response of materials in high-deformation processes. Excessive element distortion in a finite-element simulation is a fundamental problem in numerical modelling of machining processes. In this study, we present a hybrid modelling approach for micro-machining of crystalline metals with the use of smoothed particle hydrodynamics and continuum finite element analysis to overcome this problem. The model is implemented in a commercial software ABAQUS/Explicit using a user-defined subroutine (VUMAT). The model is used to elucidate the effect of crystallographic anisotropy on a response of face centred cubic (f.c.c.) metals to machining. Based on our study, cutting in the (100) plane is least sensitive to the cutting direction with (101) plane being the most sensitive. The maximum cutting force is observed to be on the (101) plane with the cutting tool oriented in the 0º.

1. Introduction

In recent years, mechanical micro-machining that includes micro-drilling, micro-cutting, micro-turning and micro-milling in the manufacture of small-sized components with complex geometries have received much attention, especially in aerospace, biomedical,

automotive and microelectronics industry. In the small scale, crystallographic anisotropy plays a crucial role in determining the overall response of a material to machining, since a magnitude of depth-of-cut is comparable to grain sizes of the material. Several experimental studies in f.c.c. metals reported on the effect of crystal orientation on chip morphology [1] and cutting forces [2-4]. Compared to the amount of available experimental data, efforts in incorporating crystal orientation into modelling of machining processes have been somewhat limited [5-8]. This is primarily due to an inherent difficulty in modelling large deformation processes at high strain rates in a numerically robust way.

Two main finite-element (FE) modelling frameworks – Lagrangian and Eulerian – have some limitations when dealing with high strains. The Lagrangian approach, where the frame of reference evolves with the material, cannot resolve large material deformations due to excessive element distortion. The Eulerian approach is unable to accurately monitor the evolving process zone which is critical in machining processes. Smoothed Particle Hydrodynamic (SPH) [9], on the other hand, is naturally adaptive and has been extensively used to study problems of multi-body dynamics and computational fluid mechanics. The SPH approach has several advantages, especially in the study of large-deformation processes. First, in SPH (that is a Lagrangian scheme) advection is treated in an exact way, which is often not the case in traditional FE methods. Also, multi-material interface problems, that are usually a challenge for traditional FE schemes, are trivial in SPH. One of the major advantages of particle methods is that they may be treated as a bridge between continuum and its fragmentation in a natural way. Finally, SPH is effective computationally since in the study of fragmentation problems calculations are carried out in the physical space where matter lies (as opposed to voids in space), thus reducing computation time and storage costs.

In this study, a hybrid modelling approach for tool penetration into a copper single crystal with based on combination of SPH and continuum finite elements is presented. The philosophy of this approach is to use a mesh-free technique in the process zone, which undergoes high strain and strain-rate deformations with material separation, with a continuum FE formulation being used for the rest of workpiece volume to reduce computational cost. To gain a physical comprehension of the cutting process at the micro

level, a material model based on crystal plasticity is implemented. Orthogonal micro-machining is studied to gain insight into the effect of crystallographic anisotropy on the response of f.c.c. cubic metals to machining. The model incorporating crystalline anisotropy is implemented in the commercial finite element software ABAQUS/Explicit using a user-defined subroutine (VUMAT). An appropriate hardening model is implemented to account for a strain-hardening behaviour of slip systems involved in the deformation process.

The paper is organized as follows. In Section 2, the fundamentals of SPH theory are summarized briefly. The theory for a crystal-plasticity model with governing equations is introduced in Section 3. In Section 4, details of the developed multi-scale finite element modelling of orthogonal cutting are explained, followed by a study of the effect of crystal orientation on the machining forces in Section 5.

2. Smoothed particle hydrodynamics

SPH is a mesh-free Lagrangian numerical method, where a set of particles is used to represent a continuum. Hydro-dynamical parameter such as pressure, velocity, density, etc. may then be tracked at these finite particles, which move with material deformation. For a given spatial distribution of these points/particles, spatial derivatives may then be evaluated without the need for an underlying grid, which is one of the major advantages of SPH. In SPH a function $f(x)$ is introduced by an integral representation [9]

$$f(x) = \int_{\Omega} f(\acute{x}) W(x - \acute{x}, h) d\acute{x} \,, \tag{1}$$

where $f(x)$ is a scalar function of the three-dimensional position vector of x, Ω is the volume of the integral that contains x, $W(x - \acute{x}, h)$ is a smoothing kernel function and h is supporting radius.

The function W satisfies the normalization condition

$$\int_{\Omega} W(x - \acute{x}, h) d\acute{x} = 1. \tag{2}$$

Also,

$$\lim_{h\to 0} W(x-\acute{x},h) = \delta(x-\acute{x}), \quad (3)$$

where $\delta(x)$ is the Dirac delta function. Finally, W satisfies the compactness condition

$$W(x-\acute{x},h) = 0, \quad (4)$$

when

$$|x-\acute{x}| > kh. \quad (5)$$

Here, k is a constant related to the smoothing function for point x and defines the effective (non-zero) area of this function known as *support domain* of that point. The continuous SPH integral representation for $f(x)$ can be written in the following form of discretized particle approximation [10]:

$$f(x_i) = \sum_{j=1}^{N} \frac{m_j}{\rho_j} f(x_i) W(x-\acute{x},h), \quad (6)$$

where m_j and ρ_j are the mass and density of the each particle, respectively. Hence, Eq. (6) states that the value of a function at particle *i* is approximated using the average of those values of the function at all the particles in the support domain of this particle weighted by the smoothing function.

The SPH computational framework is available in ABAQUS/Explicit and was readily used in our study. Within the same model, developed in ABAQUS, discrete particles and solid elements may be coupled with a kinematic tie contact algorithm that allows stable computations without distortion.

3. Crystal plasticity

A crystal-plasticity (CP) formalism was used in both SPH and continuum FE domains to model a deformation behaviour of a single-crystal metal. In the Schmid law-based CP constitutive model, the stress rate $\dot{\sigma}_{ij}$ is related to the elastic strain rate $\dot{\varepsilon}^{\mathrm{e}}_{kl}$ as:

$$\dot{\sigma}_{ij} = C_{ijkl}\dot{\varepsilon}^{\mathrm{e}}_{kl} = C_{ijkl}\left(\dot{\varepsilon}_{ij} - \dot{\varepsilon}^{\mathrm{p}}_{kl}\right), \quad (7)$$

where $\boldsymbol{C}$ is the fourth-order elasticity tensor and $\dot{\varepsilon}_{ij}$ and $\dot{\varepsilon}_{kl}^{\mathrm{p}}$ are the total strain rate and plastic strain rate, respectively, where the latter is introduced as

$$\dot{\varepsilon}_{ij}^{\mathrm{p}} = \sum_{\alpha=1}^{N} \mu_{ij}^{\alpha} \dot{\gamma}^{\alpha}. \tag{8}$$

In Eq. (8), N is the total number of available slip systems, μ_{ij}^{α} is the Schmid tensor and equals to a dyadic product of the slip direction $\boldsymbol{s}_i^{\alpha}$ and the slip plane normal $\boldsymbol{n}_j^{\alpha}$ in the initial unloaded configuration, $\dot{\gamma}^{\alpha}$ is the shear strain rate in a slip system α.

The viscoplastic power-law expression proposed by Hutchinson [11] was used to describe $\dot{\gamma}^{\alpha}$ in the following form:

$$\dot{\gamma^{\alpha}} = \dot{\gamma}_0 \operatorname{sgn}(\tau^{\alpha}) \left| \frac{\tau^{\alpha}}{g^{\alpha}} \right|^{n}, \tag{9}$$

where $\dot{\gamma}_0$ is the reference strain rate, τ^{α} is the resolved shear stress on the slip system α, obtained by the Schmid law ($\tau^{\alpha} = \sigma_{ij}\mu_{ij}^{\alpha}$), n is the material's rate sensitivity, $\operatorname{sgn}(*)$ is the signum function of $*$ and g^{α} is the strength of the slip system α at the current time, which equals to a sum of the critical resolved shear stress (CRSS) and the evolved slip-resistance due to strain hardening:

$$g^{\alpha} = g^{\alpha}|_{t=0} + \Delta g^{\alpha}, \tag{10}$$

where

$$\Delta g^{\alpha} = \sum_{\beta=1}^{N} h_{\alpha\beta} \Delta\gamma^{\beta}, \mathrm{CRSS} = g^{\alpha}|_{t=0}. \tag{11}$$

The hardening moduli $h_{\alpha\beta}$ in Eq. (11) are evaluated using the hardening model proposed by Peirce *et al*. [12] as follows:

$$h_{\alpha\alpha} = h(\gamma) = h_0 \operatorname{sech}^2 \left| \frac{h_0 \gamma}{g_{\mathrm{T}}^{\alpha}|_{\mathrm{sat}} - g_{\mathrm{T}}^{\alpha}|_{t=0}} \right|, \tag{12}$$

$$h_{\alpha\beta} = q h_{\alpha\alpha} (\alpha \neq \beta), \qquad \gamma = \sum_{\alpha} \int_{0}^{t} |\dot{\gamma}^{\alpha}| dt \,,$$

where h_0 is the initial hardening parameter, q is the latent hardening ratio and assumed to be 1, γ is the Taylor cumulative shear strain on all slip systems and $g_{\mathrm{T}}^{\alpha}|_{t=0}$ and $g_{\mathrm{T}}^{\alpha}|_{\mathrm{sat}}$ are the shear stresses at the onset of yield and the saturation of hardening, respectively.

In a f.c.c. single crystal of copper, slips may occur on 12 individual slip systems, where the slip plane is of type (111) and the slip direction is of type [110]. Material parameters used in the FE simulations are listed in Table 1, where each slip system assumed to have the same values of plastic parameters.

Table 1.

4. FEM/SPH model of orthogonal cutting

A 3D workpiece with dimensions of 500 μm × 500 μm × 50 μm was selected as an appropriate representation of a crystalline continuum. The workpiece was divided into two regions; one representing the SPH domain (200 μm × 200 μm × 50 μm) and the remaining part being a continuum FE domain (Fig. 1(a)). The FE domain was meshed with eight-node brick elements with reduced integration (C3D8R) while the PC3D element type was used to represent the SPH area. Based on an initial mesh-sensitivity analysis, the optimum number of particles in the SPH domain was determined to be 65536. In the continuum FE domain, a mesh with a minimum element size of 3.125 μm was sufficient to characterize accurately the machining process. A fixed boundary condition was imposed on the bottom and right-hand face of the workpiece (Fig 1b). A tool rake angle was 0° and a clearance angle 5º. A depth of cut was set at 10 μm, and the tool moved in the positive x direction with a velocity of 1300 mm/s. The maximum cutting length of 120 μm was considered in the simulations.

Fig. 1.

It is well known that spurious ‘ghost’ forces often get introduced when modelling domains of different scales [14]. In our model, there is no explicit characterisation of

length scales, and the underlying physics in both the SPH and FE domains is the same. Nevertheless, we evaluate the validity of the developed model by checking consistence of computed fields at the interface of the two domains. Figure 2 demonstrates the distribution of von Mises stresses along the vertical (A-B-C) and horizontal (D-E-F) paths in the entire domain at the maximum cutting length. It is observed that at points B and E, representing the boundary between SPH and FE domains, the stress values are continuous without any abrupt change (only with some small-scale fluctuations) proving that the modelled domains are appropriate. The workpiece was modelled as a deformable body and the tool a rigid body. The Coulomb's law of friction with a co-efficient of friction of $\mu = 0.12$ was used to model the frictional interaction between the tool and the workpiece material. The spatial proximity of cutting edge to the domain interface which could potentially cause some untoward issues with numerics, i.e. stability or consistency problems, needs to be checked and will be the subject of a future publication. For continuous machining problems, the SPH domain should be extended to span the entire workpiece length to take advantage of the ease of modelling material separation in the form of chips.

Fig. 2.

5. Effect of crystal orientation: Variation of cutting force and chip morphology

To study the influence of cutting direction and crystallographic orientation on the cutting forces, three cutting directions on three crystal orientations were chosen. In our analysis, a planar configuration was used, in which the tool cuts along a particular crystal direction [hkl] on a chosen crystal plane [abc] (Fig. 3).

Appropriate crystal orientations were selected such that the cutting operation was carried out on the (100), (101) and (111) planes. Three cutting directions were chosen for each cutting plane: 0º, 30º and 90º. The corresponding cutting direction and orientations used are listed in Table 2.

Fig. 3.

Table 2.

Evolution of the calculated cutting forces with an increasing cutting length for the 0º cutting direction is shown in Fig. 4. The effect of crystal orientation is evident from the character of this evolution. Initial stages of the tool-workpiece interaction (depicted as Section I in Fig. 4) demonstrate a marked difference for different crystal orientations. With increasing tool penetration the workpiece material rearranged when the strain energy in the deformed lattice exceeded the binding energy of particles. On the other hand, when the primary shear stress generated by the intrusion of the cutting tool was larger than the critical shear stress of single-crystal copper, slips would be generated in the lattice to release the strain energy. The value of shear angle can be estimated based on the Schmid's law. During micro-cutting, oscillations of the shear angle due to grain rotation resulted in variation in the observed cutting forces (Fig. 3). The level of fluctuations was less than 8% of the maximum cutting force for the (100) plane, where the finer lamellar slip structure occurred; it was approx. 20% for the (101) and (111) planes, where the coarser lamellar slip type occurred. A comparison of chip morphologies after machining showed a distinct change in the type of chip formed when moving from one direction cutting setup to another. The character of fluctuations in the cutting force was found to correspond fairly well to the pattern of the chip formation. Generation of a spatial angle of chip formation in the workpiece highlighted the importance of 3D formulation for simulation of the machining process in the single crystal of copper to account for realisation of deformation processes for various orientations of the cutting system.

Fig. 4.

Interestingly, the chip morphology is heavily influenced by crystallographic orientation as shown in Fig. 5. In our study, continuous chips with different chip morphologies were produced for all orientations. As the tool moved forward (Section I), the chip in the (101) orientation exhibited a larger thickness when compared to other two orientations. This phenomena, in turn, led to a higher maximum value of cutting force for this orientation.

In chip formation, there is a small region, in which the high strain and high strain-rate deformation process occur. Machinability of materials is often described by the shear angle. A large shear angle is associated with continuous chip formation, good surface

finish and low cutting forces. Observations of a smaller chip structure in the (100) plane compared to (111) in Section I with a higher amount of force is due to the shear angle. In the (100) orientation, the material is not amended to machining at the beginning of the process resulting in an approximately zero shear angle. When the tool moved forward (Sections II and III), the shear angle increased with a reduction in the cutting force.

Fig. 5.

Fig. 6 shows the calculated average values of cutting forces in Section III (Fig. 5) for the single-crystal of copper for different combinations of planes and cutting directions. The first observation is that for all the planes the 0° direction is characterized by the maximum value of the average force value. On the other hand, the variation in the average cutting force values for the (100) plane is smaller than that for other planes due to a basic symmetric structure of the f.c.c crystal in this plane, where this can reach the level of up to 33% (on the (101) plane), a significant value for the micro-cutting process.

Fig. 6.

In Table 3, the calculated cutting forces normalised to the cutting force in the 0° direction, are compared with experiments of Zhou and Ngoi [15]. The results of our modelling efforts are in good agreement with experimental data. From numerical studies carried out elsewhere [16], a strong dependence of the tool-nose radius on the cutting force especially was found for ultra-small cutting depths, with forces observed to change by up to 200% with a changing nose radius. Exact comparisons of cutting forces to the experiments in [15] are not possible, since the tool-tip radius used in the experimental study was significantly larger (0.5 mm) than the one used in our analysis.

Table 3.

6. Concluding remarks

A combination of SPH and continuum finite-elements approaches in a single model of a micro-machining process of crystalline copper as presented in this paper is a viable and numerically robust way for solving large-deformation problems at small length scales without compromising complex underlying physical mechanisms that drive deformation in crystalline materials.

The importance of grain orientation and direction of machining on the overall cutting forces, chip morphology was demonstrated together with propensity of the workpiece material to generate slips when its grains undergo rotations.

Between three selected grain orientations in f.c.c. single crystals – [100], [101] and [111] – the cutting-force variation on the (101) plane was observed to be larger than that on two other planes. The total difference in force for the chosen orientations was 33%, signifying the strength of the effect of crystal orientation in micro-machining process.

Acknowledgement

AZ and MD acknowledge the use of the UMAT in the development of the VUMAT for the CP theory developed by Yonggang Huang [17] and Jeffrey Kysar [18]. MD, AR and VVS acknowledge the funding from the European Union Seventh Framework Programme (FP7/2007-2013) under Grant Agreement No. PITN-GA-2008-211536, project MaMiNa.

References

[1] K. Ueda, K. Iwata, K. Nakajama, Chip formation mechanism in single-crystal cutting β-Brass, Annual CIRP – Manufacturing Technology, 29 (1) (1980) 41–46.

[2] L. B. Lawson, N. Kota, O. B. Ozdoganlar, Effects of crystallographic anisotropy on orthogonal micromachining of single-crystal aluminum, Journal of Manufacturing Science and Engineering, 130 (2008) 031116-1.

[3] S. To, WB Lee, CY Chan, Ultra-precision diamond turning of aluminum single crystals, Journal of Materials Processing Technology, 63 (1997) 157–62.

[4] N. Kota, O. B Ozdoganlar, Orthogonal machining of single-crystal and coarse-grained aluminium, Journal of Manufacturing Processes, 14 (2) (2012) 126–134.

[5] H.M. Pen, Y.C. Liang, X.C. Luo, Q.S. Bai, S. Goel, J.M. Ritchie, Multiscale simulation of nanometric cutting of single crystal copper and its experimental validation, Computational Materials Science, 50 (12) (2011) 3431-3441.

[6] R. Komanduri, N. Chandrasekaran, L.M. Raff, Orientation effects in nanometric cutting of single crystal materials an MD simulation approach, Annals of CIRP-Manufacturing Technology, 48 (1) (1999) 67–72.

[7] E. Demir, Taylor-based model for micro-machining of single crystal fcc materials including frictional effects—Application to micro-milling process, International Journal of Machine Tools & Manufacture, 48 (2008) 1592–1598.

[8] N. Kotaa, O.B. Ozdoganlar, A model-based analysis of orthogonal cutting for single crystal fcc metals including crystallographic anisotropy, Machining Science and Technology, 14(1) (2010) 102–127.

[9] J. J. Monaghan, Smoothed particle hydrodynamics, Reports on progress in physics, 68 (8) (2005) 1703-1759.

[10] Y. Chen, S. Kulasegaram, Numerical modelling of fracture of particulate composite using SPH method, Computational Materials Science, 47 (1) (2009) 60-70.

[11] J. Hutchinson, Bounds and self-consistent estimates for creep of polycrystalline materials, Proceedings of the Royal Society of London. A. Mathematical Physical & Engineering Sciences, 348 (1976) 101-127.

[12] D. Peirce, R.J. Asaro, A. Needleman, An analysis of nonuniform and localized deformation in crystalline solids, Acta Metallurgica, 30 (1982) 1087.

[13] Y. Wang, D. Raabe, C. Kluber, Orientation dependence of nanoindentation pile-up patterns and of nanoindentation microtextures in copper single crystals, Acta Materialia 52 (2004) 2229–2238.

[14] V.B. Shenoy, R. Miller, E.b. Tadmor, D. Rodney, R. Phillips, M. Ortiz, An adaptive finite element approach to atomic-scale mechanics—the quasicontinuum method, Journal of the Mechanics and Physics of Solids 47(1999) 611–642.

[15] M. Zhou, B. K. A. Ngoi, Effect of tool and workpiece anisotropy on microcutting processes, Proceedings of the Institution of Mechanical Engineers, Part B: Journal of Engineering Manufacture 215 (2001) 13–19.

[16] K.S. Woon, M. Rahman, F.Z. Fang, K.S. Neo, K. Liu, Investigations of tool edge radius effect in micromachining: A FEM simulation approach, Journal of materials processing technology 195 (2008) 204–211.

[17] Y. Huang, A user-material subroutine incorporating single crystal plasticity in the ABAQUS finite element program, Mech Report. 178 (1991).

[18] J. Kysar, Addendum to 'A user-material subroutine incorporating single crystal plasticity in the ABAQUS finite element program: Mech Report 178', Division of Engineering and Applied Sciences, Harvard University, Cambridge, MA (1997).

Table and Figure captions

Table 1. Material parameters of single-crystal copper [13]

Table 2. Cutting direction setup

Table 3. Cutting forces normalised to cutting direction of 0°

Fig. 1. (a) Tool and workpiece dimensions (in μm); (b) 3D finite-element/SPH model of micro-machining

Fig. 2. Distributions of Von Misses stress along two paths in workpiece material in (100) plane

Fig. 3. Orientations in modelling of machining

Fig. 4. Evolution of cutting forces for different cutting planes of 0º cutting direction

Fig. 5. Chip morphologies in three planes (100), (101) and (111) in 0° cutting direction for different stages of machining (Sections I – III, see Fig. 4)

Fig. 6. Typical variation of cutting force for various cutting directions

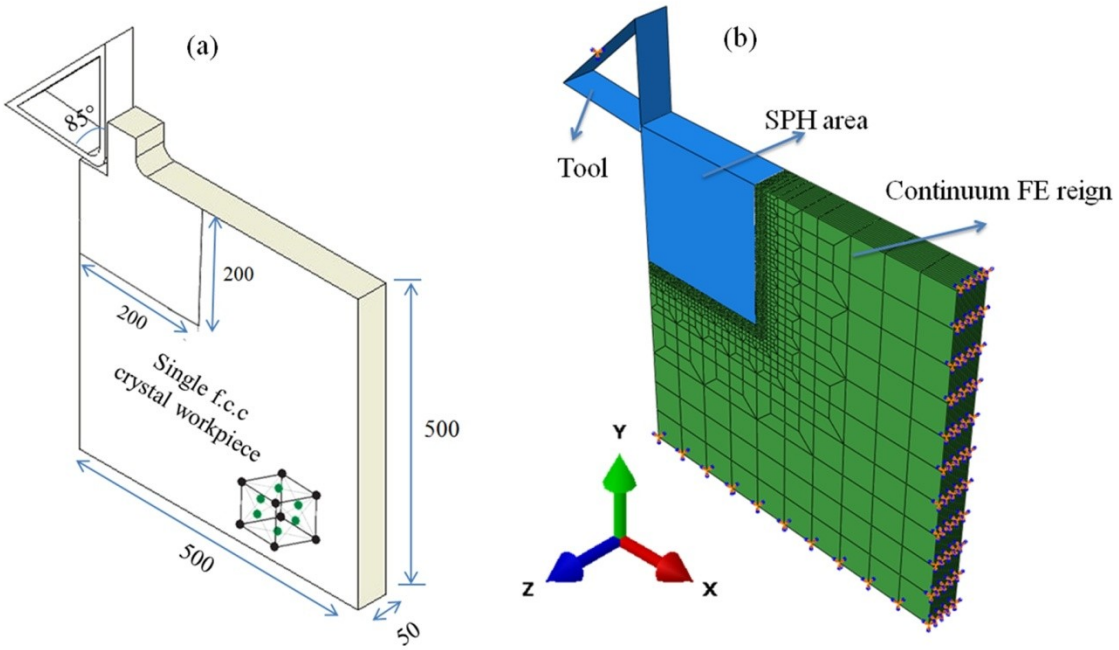
(a)
85°
200
200
Single f.c.c
crystal workpiece
500
500
50
(b)
Tool
SPH area
Continuum FE reign
Y
Z
X

Fig 1

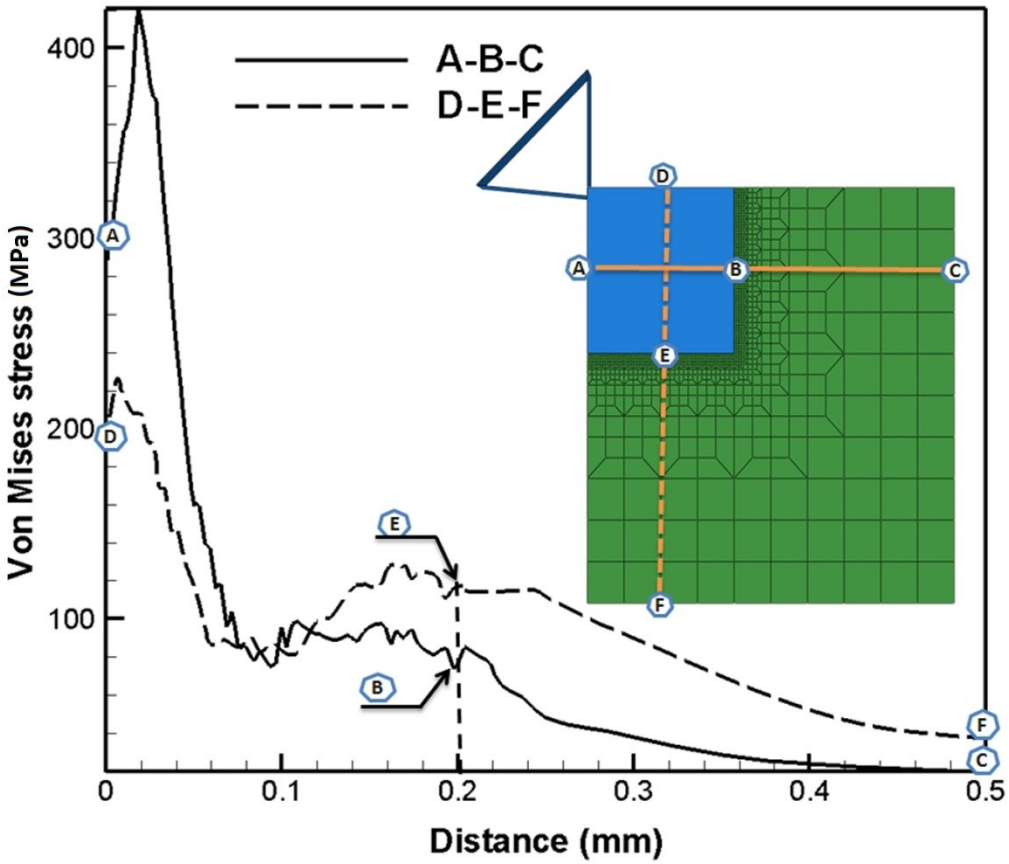
A-B-C
D-E-F
Von Mises stress (MPa)
Distance (mm)
400
300
200
100
0
0.1
0.2
0.3
0.4
0.5
A
B
C
D
E
F

Fig 2

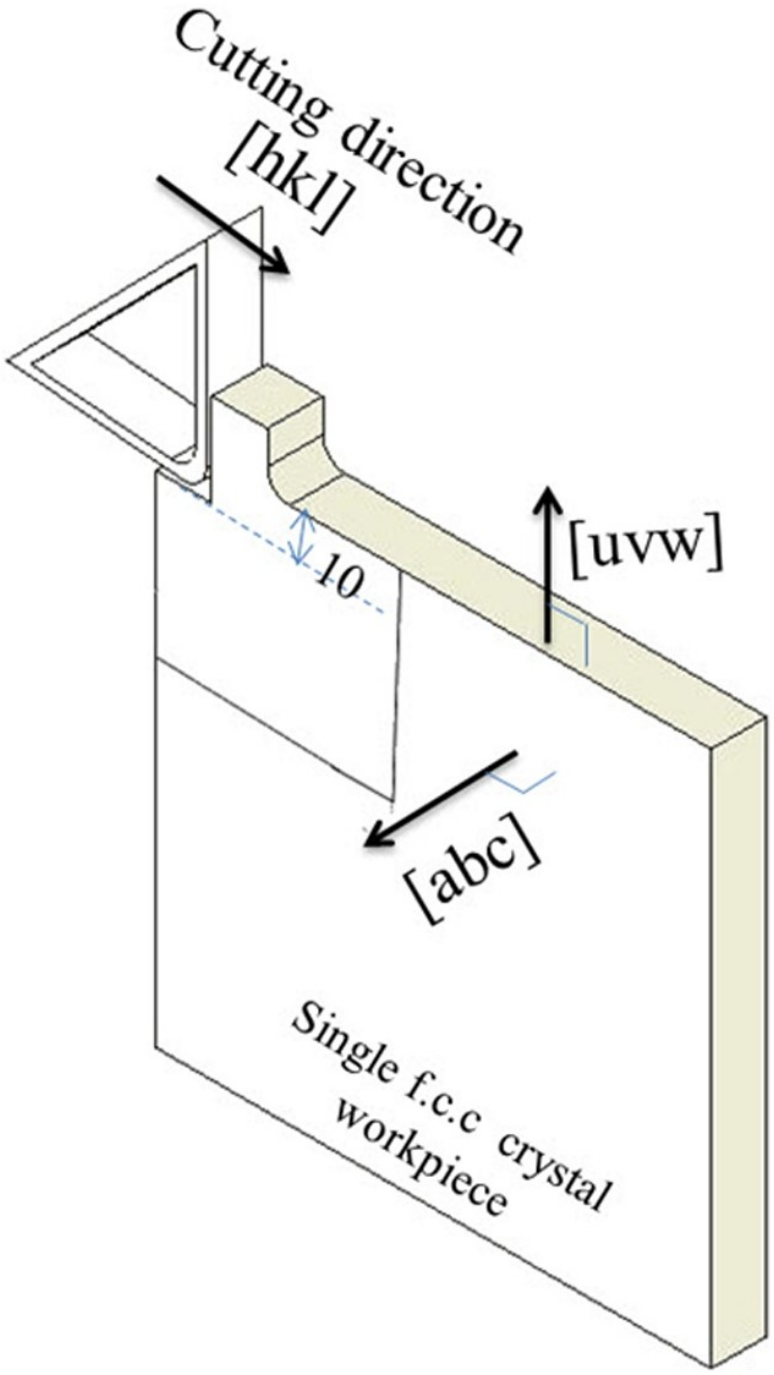
Cutting direction
[hkl]
[uvw]
10
[abc]
Single f.c.c crystal
workpiece

Fig 3

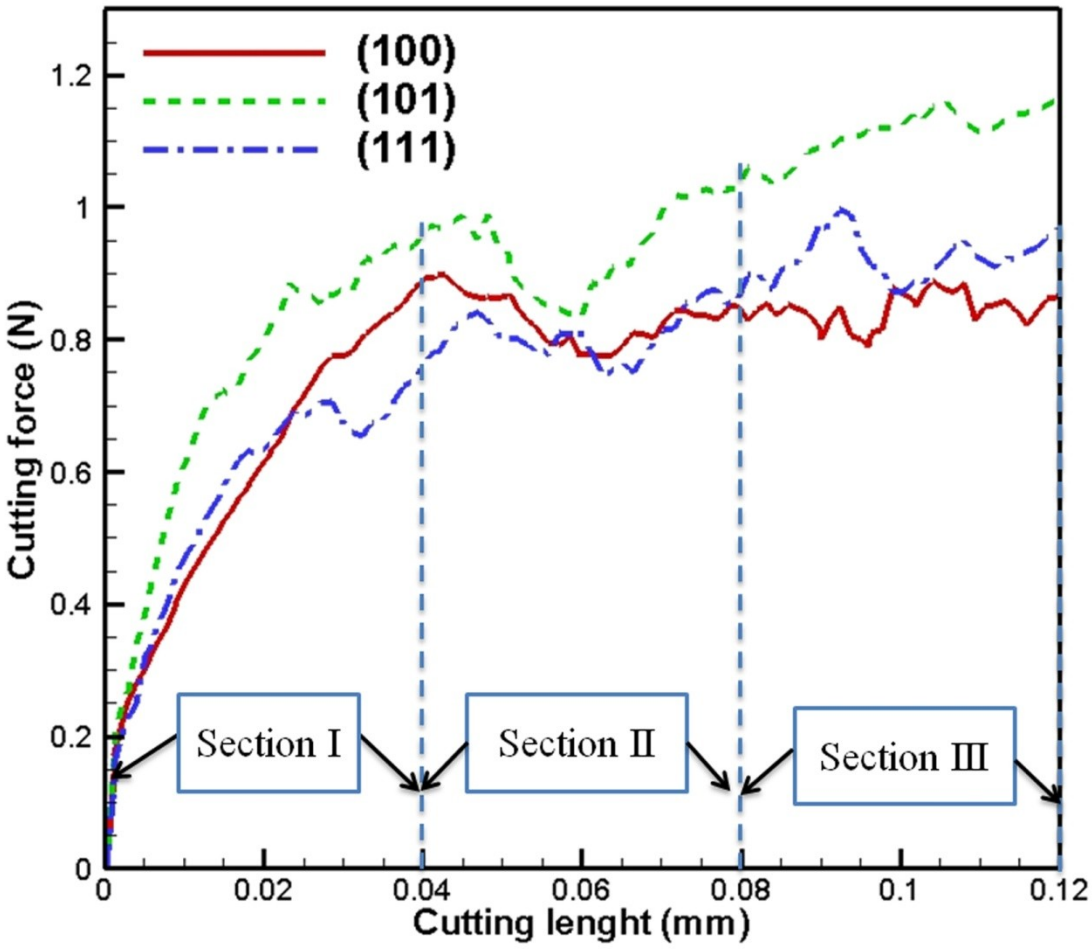
(100)
(101)
(111)
Cutting force (N)
Cutting lenght (mm)
Section I
Section II
Section III
0
0.2
0.4
0.6
0.8
1
1.2
0.02
0.04
0.06
0.08
0.1
0.12

Fig 4

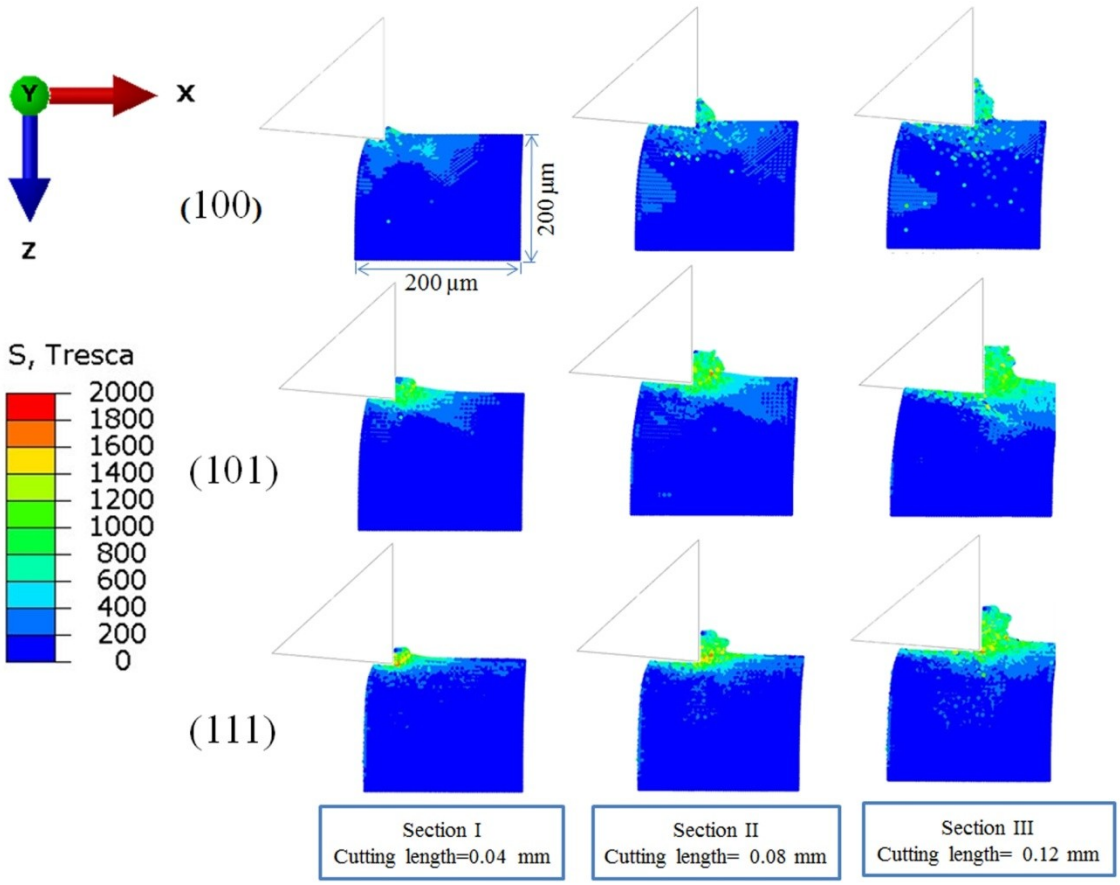
Y
X
Z
(100)
200 µm
200 µm
S, Tresca
2000
1800
1600
1400
1200
1000
800
600
400
200
0
(101)
(111)
Section I
Cutting length=0.04 mm
Section II
Cutting length= 0.08 mm
Section III
Cutting length= 0.12 mm

Fig 5

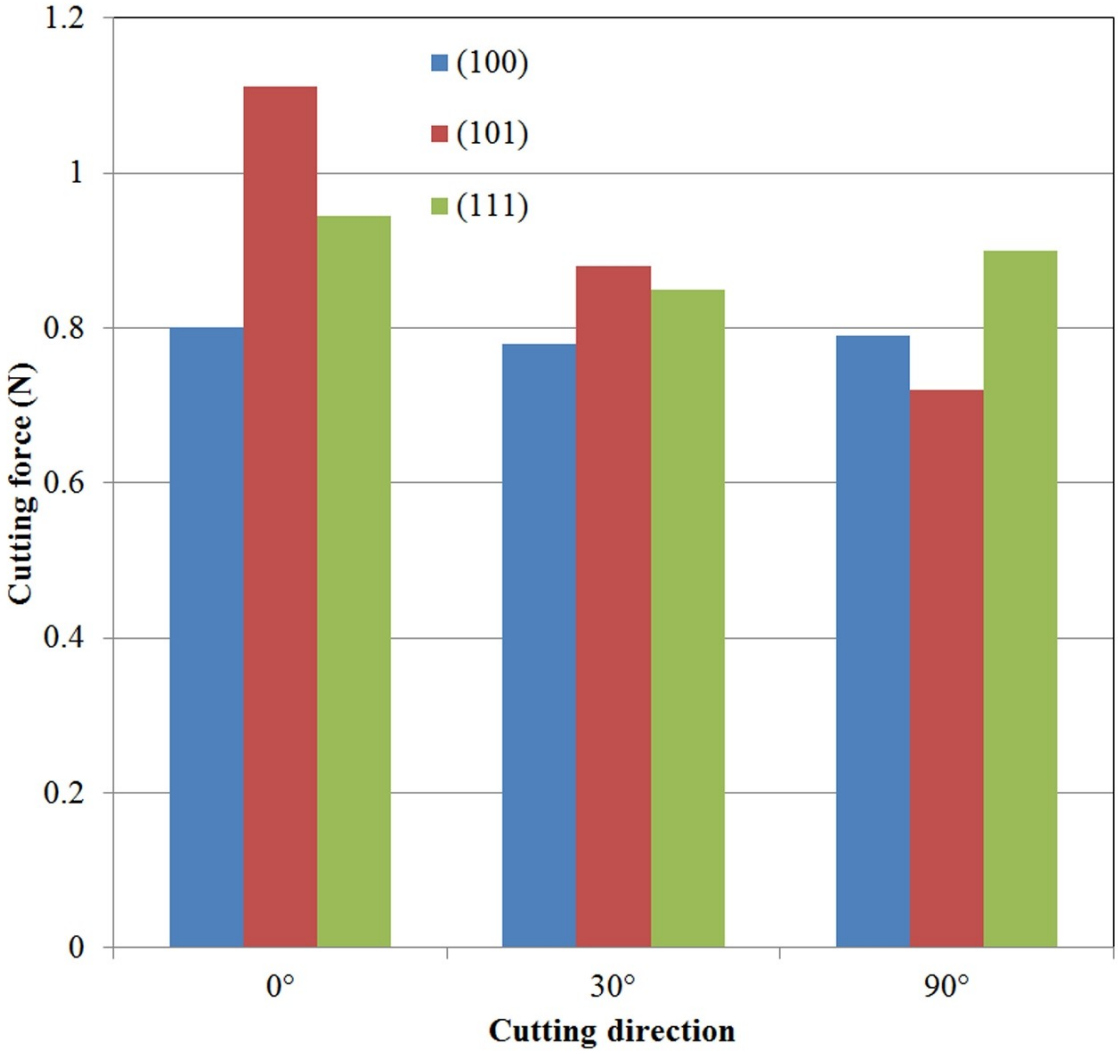
1.2
1
0.8
0.6
0.4
0.2
0
Cutting force (N)
(100)
(101)
(111)
0°
30°
90°
Cutting direction

Fig 6

Table 1. Material parameters of single-crystal copper [13]

Elastic parameters	Parameters of slipping rate	Hardening parameters
$C_{11} = 168$ GPa	$\dot{\gamma}_0 = 0.001\,\mathrm{s}^{-1}$	$h_0 = 180$ MPa
$C_{12} = 121.4$ GPa	$n = 20$	$\tau_s = 148$ MPa
$C_{44} = 75.4$ GPa		$\tau_0 = 16$ MPa

Table 2. Cutting direction setup

	0°		**30°**		**90°**	
[u v w]	**[a b c]**	**[h k l]**	**[a b c]**	**[h k l]**	**[a b c]**	**[h k l]**
[1 0 0]	[0 0 1]	[0 1 0]	[0 1 $\sqrt{3}$]	[0 $\sqrt{3}$ $\bar{1}$]	[0 1 0]	[0 0 $\bar{1}$]
[1 0 1]	[$\bar{1}$ 0 1]	[0 1 0]	[$\bar{3}\sqrt{6}$ 3]	[1 $\sqrt{6}$ $\bar{1}$]	[0 1 0]	[1 0 $\bar{1}$]
[1 1 1]	[$\bar{1}$ 0 1]	[$\bar{1}$ 2 $\bar{1}$]	[$\bar{1}$ $\bar{1}$ 2]	[$\bar{1}$ 1 0]	[$\bar{1}$ 2 $\bar{1}$]	[1 0 $\bar{1}$]

Table 3. Cutting forces normalised to cutting direction of 0°

Cutting plane	Cutting direction		
		30°	90°
(101)	Experimental	0.8014	0.6501
	Modelling	0.7927	0.6486
(111)	Experimental	0.9090	0.9354
	Modelling	0.8996	0.9425